First Crystal Structures of Human Carbonic Anhydrase II in Complex with Dual Aromatase−Steroid Sulfatase Inhibitors[†,‡]

Matthew D. Lloyd,[*,§] Nethaji Thiyagarajan,[||] Yaik T. Ho,[⊥] L. W. Lawrence Woo,[§,@] Oliver B. Sutcliffe,[§,@] Atul Purohit,[⊥] Michael J. Reed,[⊥] K. Ravi Acharya,[||] and Barry V. L. Potter[§,@]

Medicinal Chemistry, Department of Pharmacy and Pharmacology, University of Bath, Claverton Down, Bath BA2 7AY, United Kingdom, Sterix Ltd., Department of Pharmacy and Pharmacology, University of Bath, Claverton Down, Bath BA2 7AY, United Kingdom, Endocrinology and Metabolic Medicine and Sterix Ltd., Imperial College, Faculty of Medicine, St. Mary's Hospital, London W2 1NY, United Kingdom, and Department of Biology and Biochemistry, University of Bath, Claverton Down, Bath BA2 7AY, United Kingdom

Received October 29, 2004; Revised Manuscript Received March 3, 2005

ABSTRACT: Carbonic anhydrase (CA) catalyzes the reversible hydration of carbon dioxide to hydrogen carbonate. The role of CA in maintaining pH balance has made it an attractive drug target for the treatment of cancer, and it has recently been implicated in the delivery of sulfamate-containing drugs. With the acceptance of steroid sulfatase as a target for hormone-dependent cancer, novel dual aromatase−steroid sulfatase inhibitors (DASIs) containing a sulfamate group are now being developed. In this study, we show that CA II is potently inhibited by several members of this class of inhibitor. The structures of CA II complexed with 4-[(4-*O*-sulfamoylbenzyl)(4-cyanophenyl)amino]-4*H*-[1,2,4]triazole ($K_D = 84 \pm 5$ nM) and 4-[(3-bromo-4-*O*-sulfamoylbenzyl)(4-cyanophenyl)amino]-4*H*-[1,2,4]triazole ($K_D = 454 \pm 29$ nM) are reported to 2.02 and 1.76 Å, respectively. Both inhibitors ligate to the active site zinc(II) atom via their sulfamate nitrogen, while the rest of the molecule is contained within the hydrophobic binding pocket. Key protein residues include Val-121, Phe-131, Val-135, Val-143, Leu-141, Leu-198, Pro-202, and Leu-204. Despite being structurally similar, the two ligands experience different types of binding particularly in the sulfamate-containing aromatic ring and the opposite geometric arrangement of the triazole and cyanophenyl groups around the configurationally invertible central nitrogen atom. Small changes in inhibitor structure can cause large changes in binding to CA II, and this underlines the importance of structure-based drug design with this enzyme and other isoforms relevant to potential anticancer therapy. Moreover, these results underpin the idea that binding to erythrocyte CA II may be a general method of stabilizing and delivering sulfamate-based drugs in vivo.

Carbonic anhydrase (CA,[1] EC 4.2.1.1) is a zinc(II)-dependent enzyme that catalyzes the reversible hydration of carbon dioxide to hydrogen carbonate and a proton. The enzyme plays an important role in physiological anion-exchange processes and fluid balance (*1*), and has long been a drug target for the treatment of glaucoma (*2*, *3*). At least 14 isoforms of CA have been identified in vertebrates with different physiological and pathological roles, and they can be localized in the cytosol (CA I−III and CA VII) or mitochondria (CA V), while others are secreted (CA VI) or are membrane-bound and have extracellular active site domains (CA IV, IX, XII, and XIV) (*3*). There is convincing evidence for overexpression of CA isoforms IX and XII in cancer (see ref *4*), and this may acidify the extracellular matrix which is thought to promote growth of the tumor. Solid tumors are often hypoxic, and expression of CA IX and XII is upregulated under these conditions (*5*, *6*). Recently, CA has become important as a potential target for obesity (*7*) and cancer (*8*, *9*). CA isoforms can catalyze a series of other hydration and dehydration reactions, although it is unclear whether these reactions have any physiological significance in normal or cancerous cells (*10*).

Breast cancer is a major cause of mortality in Western countries, with a lifetime risk of 1:9. The majority of tumors occur in post-menopausal women, who have nonfunctional ovaries, with estrogens produced in peripheral tissues. Many tumors are initially estrogen-dependent, with the hormones supporting their growth and development. Established mainstream therapies for hormone-dependent breast cancer (HDBC) involve either antagonizing estrogen receptor activity with selective estrogen receptor modulators (e.g., tamoxifen) or reducing levels of estrogens using aromatase inhibitors. Aromatase is a cytochrome P450 (CYP) monooxygenase that

[†] This work was funded by Sterix Ltd. as a member of the Ipsen group.

[‡] The atomic coordinates have been deposited in the Protein Data Bank as entries 1XPZ and 1XQ0.

* To whom correspondence should be addressed. Phone: +-44-1225-386786. Fax: +-44-1225-386114. E-mail: M.D.Lloyd@bath.ac.uk.

[§] Medicinal Chemistry, Department of Pharmacy and Pharmacology, University of Bath.

[||] Department of Biology and Biochemistry, University of Bath.

[⊥] St. Mary's Hospital.

[@] Sterix Ltd., Department of Pharmacy and Pharmacology, University of Bath.

[1] Abbreviations: CA II, human carbonic anhydrase II; DASI, dual aromatase−steroid sulfatase inhibitor; DMSO, dimethyl sulfoxide; EMATE, estrone-3-*O*-sulfamate; IPTG, isopropyl β-D-thiogalactopyranoside; MeCN, acetonitrile; STS, steroid sulfatase.

10.1021/bi047692e CCC: $30.25
Published on Web 04/16/2005

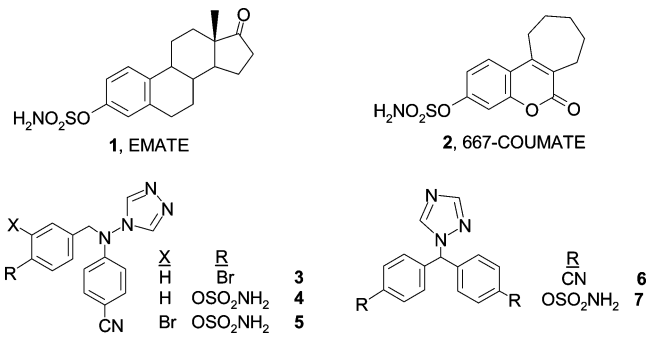

FIGURE 1: Structures of EMATE (**1**), 667COUMATE (**2**), YM511 (**3**), letrozole (**6**), and DASI inhibitors **4**, **5**, and **7**.

catalyzes conversion of androgens to estrogens. Inhibitors can be either irreversible (e.g., exemestane and formestane) or tight-binding reversible inhibitors (e.g., anastrozole and letrozole). All potent reversible aromatase inhibitors invariably contain a heme-chelating azole ring such as triazole. A second important enzyme in the production of estrogens in tumors is steroid sulfatase (STS),[1] which can be irreversibly inhibited by estrone-3-*O*-sulfamate (EMATE) (Figure 1, **1**). This enzyme is now a recognized oncology target, and its role in HDBC is currently being investigated in a Phase 1 clinical trial of the nonsteroidal inhibitor 667COUMATE (Figure 1, **2**) (*11*), the first sulfamate-based STS inhibitor to be administered to humans. It has been reasoned that inhibitors of STS given in conjunction with aromatase inhibitors should maximize estrogen depletion in treated patients.

While administering an STS inhibitor in conjunction with an aromatase inhibitor is an obvious approach, an alternative approach is to design a dual aromatase−steroid sulfatase inhibitor (DASI) that will inhibit both enzymes as a single agent. Recently, we validated the feasibility of the DASI concept, by adopting a strategy where the required pharmacophore for STS inhibition is incorporated into two established aromatase inhibitors, the developmental agent YM511 (Figure 1, **3**) and the clinically used letrozole (Figure 1, **6**). Important examples of new DASI inhibitors include 4-[(4-*O*-sulfamoylbenzyl)(4-cyanophenyl)amino]-4*H*-[1,2,4]triazole (Figure 1, **4**) (*12*) and 4-[(3-bromo-4-*O*-sulfamoylbenzyl)-(4-cyanophenyl)amino]-4*H*-[1,2,4]triazole (Figure 1, **5**) (*12*) which are YM511 **3** derivatives, and 1-[bis(4-sulfamoyloxyphenyl)methyl]-1*H*-[1,2,4]triazole (*13*) (Figure 1, **7**), which is structurally related to letrozole **6**. Compound **5** contains a bromine atom substituted ortho to the sulfamate group which renders **5** more potent than its unsubstituted congener **4** against both aromatase ($IC_{50} = 0.82 \pm 0.3$ and 100 ± 7.8 nM, respectively) and STS ($IC_{50} = 39 \pm 4.2$ and 227 ± 28 nM, respectively) in a JEG-3 cell preparation (*12*). Both compounds have been shown to be active in vivo in female Wistar rats with compound **5**, at a single 10 mg/kg oral dose, reducing plasma estradiol levels to the same extent as YM511 and inhibiting STS activity almost completely 3 h after drug administration (*12*).

Estrone-3-*O*-sulfamate (EMATE) is the benchmark irreversible sulfamate-based steroid sulfatase (STS) inhibitor (Figure 1, **1**) (*14*−*16*). Recently, it has been demonstrated that two potent inhibitors of STS, EMATE (*8*, *9*, *17*) and the nonsteroidal 667COUMATE (Figure 1, **2**) (*8*, *17*), are inhibitors of human CA II in vitro and are transported in erythrocytes complexed to CA II. In the case of 667COUMATE **2**, this complexation confers increased in vivo drug stability and protection from first-pass metabolism (*18*), contributing to the excellent bioavailability of 95% observed for this STS inhibitor in rodents. To further demonstrate the association of 667COUMATE with CA II, the molecular details of binding to CA II have been determined by X-ray crystallography (*19*). It is of interest to examine whether the more diverse DASI structures could also bind to CA II through their sulfamate group and whether this might also form the basis for selective delivery and transport in vivo. We report here the X-ray crystal structures of human carbonic anhydrase complexed with **4** and **5** at 2.02 and 1.76 Å, respectively, together with the in vitro CA II inhibition and stability studies for these novel agents.

EXPERIMENTAL PROCEDURES

Materials. All chemicals and reagents were purchased from the Sigma-Aldrich Chemical Co. or Fisher Ltd., were analytical grade or higher, and were used without further purification. Plasmid pACA encoding human CA II (*20*) was obtained from Professor C. Fierke (University of Michigan, Ann Arbor, MI) and cells were grown and protein purified as previously described (*19*). Inhibitors **4**−**7** (Figure 1) were synthesized as previously described (*12*, *13*). Amersham Biosciences provided protein chromatography systems and columns.

Stability Study of Inhibitors by HPLC. Decomposition of inhibitors to their respective phenolic products was studied by dissolving ca. 1 mg of each inhibitor in 0.7 mL of a DMSO/MeCN mixture (75:25) and incubating them at room temperature (22 °C). Aliquots, in duplicate, were removed at intervals, and the remaining inhibitor was quantified by HPLC using a Waters 717 system with an autosampler and PDA detector under the following conditions: Waters "Symmetry" C18 column (3.5 μm packing, 4.6 mm × 150 mm); elution for 667COUMATE, MeCN/H_2O (90:10, isocratic, 1 mL/min); elution for **4**, MeCN/H_2O (55:45, isocratic, 1 mL/min); elution for **5** (gradient), MeCN/H_2O (5:95, 0.7 mL/min) to MeCN/H_2O (95:5, 1.4 mL/min) over 9 min followed by isocratic elution under the final conditions for a further 5 min.

Assays and Measurement of IC_{50} Values and Dissociation Constants. Inhibition constants (IC_{50} values) were measured as previously described (*8*), using a 96-well plate spectrophotometric assay. Assays contained human CA II (Sigma, 7 units/mL) and 1 mM 4-nitrophenyl acetate in 50 mM Tris-HCl (pH 7.8) in a final volume of 0.18 mL and were incubated for 20 min at 20 °C. Stock solutions of inhibitors were prepared in tetrahydrofuran, and four replicants at each concentration were used.

Inhibitor dissociation constants for **4** and **5** were determined as previously described using the purified recombinant enzyme (*19*). Final concentrations of the enzyme and 4-nitrophenol acetate substrate in the assay were 87 nM and 2.95 mM, respectively. The activity of the enzyme in the absence of any inhibitor was 3.43 μmol min^{-1} mg^{-1}. Final concentrations of **4** and **5** in the assays were 33, 83, 166, 250, and 333 nM and 166, 333, 500, 666, and 833 nM, respectively.

Crystallization, Data Collection, and Structural Determination. Crystallizations used the hanging drop vapor diffusion

Table 1: IC_{50} Values for Various Inhibitors of Human CA II, Aromatase, and STS[a]

inhibitor	IC_{50} (nM) for CA II (this study)	IC_{50} (nM) for aromatase	IC_{50} (nM) for STS
EMATE **1**	23 ± 12	ND[c,e]	25[b]
667COUMATE **2**	22 ± 4	300 ± 42[c]	1.5 ± 0.3[c]
3	>1000	0.5 ± 0.03[d]	ND[e]
4	27 ± 8	100 ± 7.8[d]	227 ± 28[d]
5	137 ± 19	0.82 ± 0.3[d]	39 ± 4.2[d]
6	>1000	0.89 ± 0.13[c]	ND[c,e]
7	22 ± 4	3044 ± 48[c]	>10000[c]

[a] Structures of the tested inhibitors are shown in Figure 1. The IC_{50} value for inhibition of CA II by EMATE, the benchmark STS inhibitor, has been reported to be 10 nM (*9*), 42 nM (*8*), and 9 nM (*17*). [b] Assayed in placental microsomes (*11*). [c] Assayed in JEG-3 cells (*13*). [d] Assayed in JEG-3 cells (*12*). [e] None detected.

method. Protein solutions (3.5 μL, ~10 mg/mL, ~0.3 mM) containing **4** or **5** (at ~0.5 mM) and 30 mM 2-mercaptoethanol was mixed with well buffer [3.5 μL; 0.1 M Tris-HCl (pH 8.0), 1 mM $ZnSO_4$, and 2.28 M ammonium sulfate for **4**; 0.1 M Tris-HCl (pH 8.0), 1 mM $ZnSO_4$, and 2.49 M ammonium sulfate for **5**], with crystals appearing after 6−8 weeks at 4 °C.

X-ray diffraction data were collected at station 14.1 at the Synchrotron Radiation Source (Daresbury, U.K.) at room temperature with a 4 s exposure and a crystal to detector distance of 100 mm (for **4**) or 70 mm (for **5**), with 1° oscillation per frame collected, ~150 images in total. Data were indexed and reduced with DENZO and SCALEPACK modules of the HKL suite (*21*) in the orthorhombic $P2_12_12_1$ space group. CA II crystallized in the $P2_12_12_1$ space group containing the active site zinc without any waters [PDB entry 1UGG (*22*), with the mutant S65 residue rebuilt as wild-type A65] was used as the starting model for rigid body refinement followed by energy minimization and isotropic thermal factor (*B*-factor) refinement within CNS 1.0 (*23*). Clear density for the inhibitor was observed in the difference map after a single round of refinement ($R_{free} = 0.26$ and $R_{cryst} = 0.24$ for **4**; $R_{free} = 0.27$ and $R_{cryst} = 0.25$ for **5**). Simulated annealing, introduction of the inhibitor, and alternating cycles of water addition, manual rebuilding within O (*24*), and energy minimization and *B*-factor refinement gave final models with the following values: $R_{free} = 0.22$ and $R_{cryst} = 0.19$ for **4** and $R_{free} = 0.21$ and $R_{cryst} = 0.19$ for **5** (Table 2). Refinement parameters for **4** and **5** were generated on the basis of the small molecule crystal structure of **5** (L. W. L. Woo, M. F. Mahon, and B. V. L. Potter, unpublished results).

RESULTS AND DISCUSSION

Stability of DASIs in DMSO. While aryl sulfamate esters in their solid form are perfectly stable, some of them degrade over time in solution to their corresponding phenolic compounds as the result of the hydrolysis of the sulfamate group (*25*), and this desulfamoylation process appears to be most prominent in highly polar solvents such as DMSO. 667COUMATE **2** is protected from degradation in vivo by complexation with CA II (*18*). Both EMATE and 667COUMATE are phenyl sulfamate esters, as are the YM511-derived DASIs. It is therefore anticipated that DASIs **4** and **5** might display similar stability characteristics of a phenyl sulfamate ester, albeit to a different degree than 667COUMATE **2** because of different physicochemical properties,

Table 2: Crystallographic Statistics of Data Collection and Refinement for the CA II−**4** and CA II−**5** Adducts

	complex with **4**	complex with **5**
data collection		
resolution range (Å)	50−2.02	50−1.76
space group	$P2_12_12_1$	$P2_12_12_1$
unit cell dimensions (Å)	42.6, 72.8, 75.2	42.6, 72.6, 75.1
highest-resolution shell (Å)	2.15−2.02	1.83−1.76
total no. of reflections	174865	292440
no. of unique reflections	15968	23147
completeness (%)[a]	98.1 (95.5)	97.0 (95.7)
R_{sym} (%)[a,b]	0.083 (0.177)	0.098 (0.392)
$I/\sigma(I)$[a]	16.4 (11.3)	17.5 (8.5)
CNS refinement		
no. of refined protein residues	3−261	3−261
no. of refined water molecules	121	172
no. of refined zinc atoms	2	2
resolution range in refinement (Å)	50−2.02	50−1.76
R_{free}[c]	0.22 (0.22, 2.02−2.06 Å)	0.21 (0.28, 1.76−1.78 Å)
test set size (%)	5.8	5.5
R_{cryst}[c]	0.19 (0.17, 2.02−2.06 Å)	0.19 (0.21, 1.76−1.78 Å)
rms deviations		
bond lengths (Å)	0.007	0.010
bond angles (deg)	1.7	1.7
average *B* value (Å^2)	27.0	24.2
primary Zn^{2+} *B*-factor (Å^2)	17.0	13.6
secondary Zn^{2+} *B*-factor (Å^2)	34.9	28.8
ligand *B*-factor range (Å^2)	34.2−55.9	19.4−31.5
water *B*-factor average (Å^2)	36.0	37.0
Ramachandran plot		
most favored (%)	88	88
additionally allowed (%)	10	11.1
generously allowed (%)	1.4	0.9
disallowed (%)	0	0

[a] Values in parentheses are for the highest-resolution shell: 2.09−2.02 Å for **4** and 1.83−1.76 Å for **5**. [b] $R_{sym} = \sum_j\sum_h|I_{j,h} - \langle I_h\rangle|/\sum_i\sum_h\langle i_h\rangle \times 100$, where $I_{j,h}$ values are intensities of symmetry redundant reflections and $\langle I_h\rangle$ is the mean intensity of reflection. [c] R_{free} and R_{cryst} are derived from CNS (*23*).

and hence, their degradation profiles should be evaluated. To this end, solutions of **4** and **5** in a mixture of DMSO and MeCN (75:25) were monitored by HPLC for the disappearance of sulfamate at room temperature (22 °C) over time. As a reference, the degradation of 667COUMATE was also assessed under identical conditions. The stability profiles of these compounds are shown in Figure 2. As anticipated, 667COUMATE is the least stable inhibitor in DMSO and MeCN at room temperature with a half-life of ca. 2 days. The half-lives of **4** and **5** were found to be significantly longer at ca. 21 and 7 days, respectively, demonstrating that these sulfamate-based DASIs are more stable than 667COUMATE. The fact that **4** was found to be more stable than **5** is in agreement with our previous observations that an aryl sulfamate whose S−O bond is weakened by an electron-withdrawing group on the aryl ring is more labile and hence more susceptible to hydrolytic cleavage (*25*, *26*). For **5**, the electron-withdrawing bromine atom ortho to the sulfamate group enhances the leaving ability of the corresponding parent phenol whose pK_a value is expected to be lower than that of the corresponding phenol of **4**. However, it is most likely this same effect that renders sulfamate **5** a more potent STS inhibitor than the nonhalogenated congener **4** by virtue of a more efficient inactivation of STS via irreversible

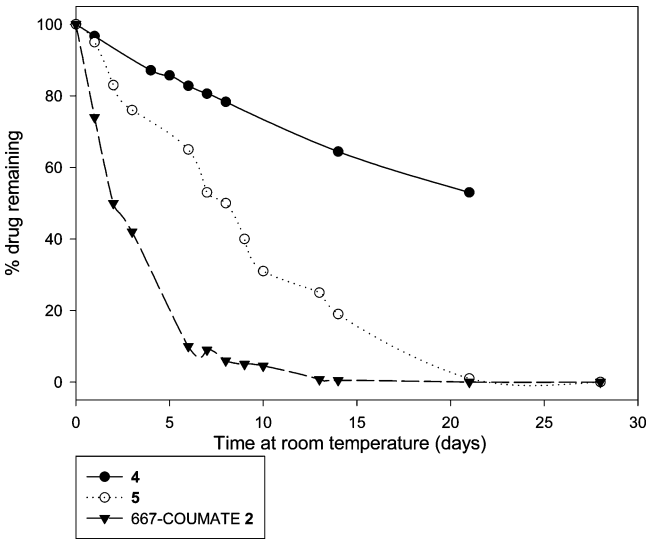

FIGURE 2: In vitro stability of 667COUMATE and sulfamates **4** and **5** in dimethyl sulfoxide and acetonitrile (75:25) at room temperature. The percentage of sulfamate remaining over time was monitored by HPLC. The λ_{max} and t_R values of the sulfamates are 290 and 311 nm and 2.28 min for 667COUMATE, 265 nm and 2.59 min for **4**, and 267.5 nm and 11.73 min for **5**, respectively. Points are the means of duplicate determinations. The standard deviation of each point is within ±2% and is not shown. Half-lives for 667COUMATE, **4**, and **5** were ca. 2, 21, and 7 days, respectively, and were estimated from plots of ln(fraction of drug remaining) vs time (not shown).

sulfamoylation of an essential amino acid residue in the enzyme active site (*11*, *15*, *25*, *26*).

Inhibition of Carbonic Anhydrase. The esterase activity of human carbonic anhydrase II was assayed using the reported spectrophotometric assay (*8*) and inhibition of activity by EMATE **1**, the benchmark inhibitor, determined. In this assay, EMATE **1** had an IC_{50} value of 23 nM (Table 1), consistent with the previously reported IC_{50} values of 42 (*8*) and 10 nM (*9*). Inhibition of activity by compounds **2**−**7** (Figure 1) was then assessed by this assay (Table 1). These results indicate that at least one sulfamate group is needed for inhibition, and this is consistent with previous results (*2*, *3*, *8*, *9*, *17*, *19*, *27*−*29*) showing that inhibition arises due to coordination of the active site zinc(II) metal atom with the inhibitor sulfamate group. Inhibitors occupy the fourth position normally occupied by the water/hydroxide ligand necessary for catalyzing hydration of CO_2 and the other carbonic anhydrase-catalyzed reactions (*10*).

Compounds **1**, **2**, **4**, and **7** had IC_{50} values in the range of 20−30 nM, while **5** was 4−5 times less potent with an IC_{50} value of 137 nM (Table 1). To further characterize this binding, the equilibrium dissociation constants for **4** and **5** were determined to be 84 ± 5 and 454 ± 29 nM, respectively. Taken together, these results confirm that **5** binds ∼5 times less potently to CA II than **4**. The relatively low IC_{50} values observed for all of the sulfamate-containing drugs indicate that binding of the carbon skeleton of the drug molecule is relatively nonspecific, and that human CA II is able to accommodate a diverse range of structures providing a zinc(II)-binding group is present. Pharmacokinetic studies have shown that 667COUMATE **2** is stabilized in whole blood relative to plasma and is protected from first-pass metabolism, and this has been ascribed to drug binding to carbonic anhydrase in erythrocytes (*18*). The IC_{50} values obtained in this study for sulfamate-containing DASIs **4**, **5**, and **7** comparable to that for 667COUMATE **2** [22 nM (Table 1); literature values of 25 (*8*) and 17 nM (*17*)] suggest that these inhibitors will also bind to carbonic anhydrase in vivo and consequently will be protected from first-pass metabolism as experienced with 667COUMATE **2**.

*Overall Structures of the **4** and **5** Complexes with Carbonic Anhydrase*. Complexes of human CA II with **4** and **5** were obtained by cocrystallization in the $P2_12_12_1$ space group. Inspection of the first maps showed strong positive density within 2.5 Å of the active site zinc(II) atom, indicating the presence of the inhibitor within the active site. Crystals were grown in the presence of zinc(II) in the crystallization solution, and a second zinc(II) atom from a symmetry-related molecule was observed at the entrance of the active site cavity. This second zinc(II) atom is involved in crystal packing interactions (*19*). Final models were produced by addition of the second zinc atom, water molecules, and inhibitor in conjunction with manual rebuilding and further refinement within CNS (Table 2). The **4** complex had a final R_{free} of 0.22 and an R_{cryst} of 0.19, and the **5** complex had a final R_{free} of 0.21 and an R_{cryst} of 0.19. The overall structures are very similar to that of CA II without any ligand bound (*22*), as judged by rms deviations for Cα atoms only of 0.23 and 0.26 Å, respectively.

As expected, both refined structures contained a zinc(II) atom ligated by the three active site histidine residues (His-94, -96, and -119) in a tetrahedral geometry (Table 3). The fourth ligand was provided by the deprotonated sulfamate group of the inhibitor, which in both cases was ligated at a distance of 2.1−2.3 Å. Although this bond distance is longer than that observed in many other crystal structures, it is very similar to that observed for the previously reported structure of the 667COUMATE **2**·CA II complex (*19*). Binding of the inhibitor is stabilized by a network of hydrogen bonding interactions, which have also been observed for the complex with 667COUMATE **2** and other inhibitors (*2*, *3*, *9*, *19*, *27*−*29*). There was no evidence for inhibitor decomposition or covalent modification of protein residues upon binding.

A second active site zinc(II) atom was incorporated into both structures (Figure 3). As previously observed (*19*), the active site zinc is ligated by His-64 and His-36 from a symmetry-related molecule. Both remaining coordination positions of the second zinc(II) atom are occupied by water molecules, unlike the 667COUMATE **2** complex in which only one water molecule is bound.

Binding of Inhibitors within the Active Site. Both **4** and **5** bind within the CA II active site by ligation of the sulfamate group to the active site zinc(II) metal atom (Figures 5 and 6). The remainder of the molecule is located within the active site funnel leading to the surface, which is lined with hydrophobic residues (Figure 3). Key residues involved in these interactions include Val-121, Phe-131, Val-135, Leu-141, Val-143, Leu-198, Pro-202, and Leu-204. The triazole and cyanophenyl groups are located in a wide funnel at the surface of the protein, which can be accessed by the solvent. This part of the molecule is relatively mobile as it has no close protein residues, although part of the symmetry-related molecule is within this region. The high mobility of this part of the ligands is reflected by their higher *B*-factors and the weaker density observed in the $2|F_o| - |F_c|$ and $|F_o| - |F_c|$ maps and $|F_o| - |F_c|$ omit maps.

Table 3: Important Interactions that Stabilize Binding of Compounds **4** and **5** to the Active Site Zinc(II) Metal Atom and Thr-199

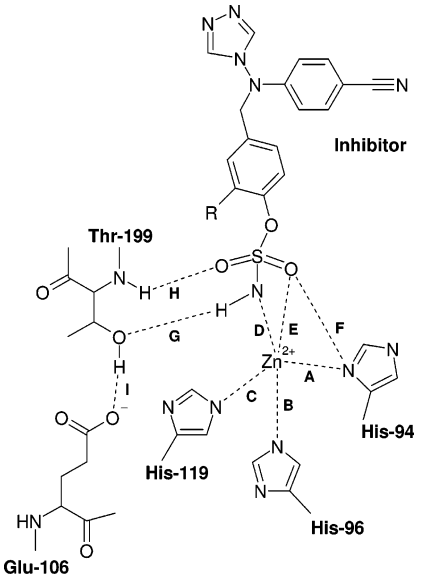

	first residue and atom	second residue and atom	distance in the **4** complex (R = H) (Å)	distance in the **5** complex (R = Br) (Å)
A	His-94 NE2	Zn	2.1	2.0
B	His-96 NE2	Zn	2.2	2.1
C	His-119 ND1	Zn	2.1	2.1
D	inhibitor SO_3NH	Zn	2.3	2.1
E	inhibitor $SO_3\overline{N}H$ O2	Zn	2.9	3.0
F	inhibitor $S\overline{O}_3NH$ O2	His-94 NE2	3.3	3.4
G	inhibitor $S\overline{O}_3NH$	Thr-199, side chain OH	2.9	2.6
H	inhibitor $SO_3\overline{N}H$ O1	Thr-199, main chain NH	3.0	3.1
I	Glu-106 $O\overline{E}1$	Thr-199, side chain $\overline{O}H$	2.7	2.7

Compounds **4** and **5** have an almost identical structure, with the latter having a bromine atom at the meta position of the aromatic ring (Figure 3). The presence of the bromine atom in **5** presumably improves the tightness of binding to aromatase and STS as well as increasing the "sulfamoylation potential" of the inhibitors toward the inactivation of STS (Table 1) (*11*, *15*), as judged by its lower IC_{50} values relative to that of **4**. Binding of the two compounds is similar within the CA II active site, but not identical. Introduction of the bromine appears to rotate the sulfamate-bearing aromatic ring by ~30° away from Val-121 and toward Pro-202, and the ring is displaced by ~1.8 Å toward Val-121 (Figures 3b and 4). This is presumably due to steric interactions between the protein and the large bromine atom. Although there are other differences in binding between the two inhibitors, these are confined mainly to the triazole and cyanophenyl groups that are located in the wide funnel at the entrance of the active site, where there is little binding of the inhibitors to the protein in this region. Thus, the positioning of the sulfamate-containing aromatic ring and accommodation of the large bromine atom appear to be the major factors that result in a significantly higher IC_{50} value for **5** in the CA II activity assay, and this is also mirrored in the K_D values.

Examination of the inhibitor conformations (panels a and b of Figure 3 and overlay in Figure 4) shows a different orientation of the groups about the central tertiary amine linker. In the case of **4** (Figure 4), the tertiary amine group has an almost flat geometry with the triazole and cyanophenyl groups arranged with *R* stereochemistry. This results in the triazole group projecting toward the symmetry-related molecule and especially residues His-36 and the second zinc(II) atom. Residues His-4 and Trp-5 from the binding CA II molecule are also located in this region (Figures 3a and 4). This triazole ring was refined with an occupancy of 0.5, suggesting that other rotamer conformations are present. The cyanophenyl group is located close to the side chains of Phe-131, Val-135, and Leu-141. The cyanophenyl ring was refined with an occupancy of 1.0, the same as for the sulfamate-bearing phenyl ring. This suggests that the low occupancy of the triazole ring is not due to a proportion of this inhibitor having *S* stereochemistry or an alternative rotation of the *R* configuration.

In contrast to the structure of the **4** complex, the stereochemistry of **5** around the central tertiary amine in its CA II complex appears to be the *S* stereoisomer, although it too has a flattened geometry. In this complex, the sulfamate-bearing ring was modeled with an occupancy of 1.0, while the triazole and cyanophenyl rings were both modeled with an occupancy of 0.7. Both the triazole ring and the cyanophenyl ring have density present in the $2|F_o| - |F_c|$ map of the **5** complex structure, and only a single stereoisomer could be modeled in this crystal structure. It is not clear whether the remaining 30% of the inhibitor has the opposite stereochemistry, or if an alternative rotamer exists. The small molecule X-ray crystal structure of **5** shows the presence of a 50:50 mixture of *R* and *S* stereoisomers (L. W. L. Woo, M. F. Mahon, and B. V. L. Potter, unpublished results), showing that binding of **5** to CA II biases the configuration of the invertible nitrogen. The cyanophenyl ring of **5** is in a position similar to that observed for **4**, while the triazole

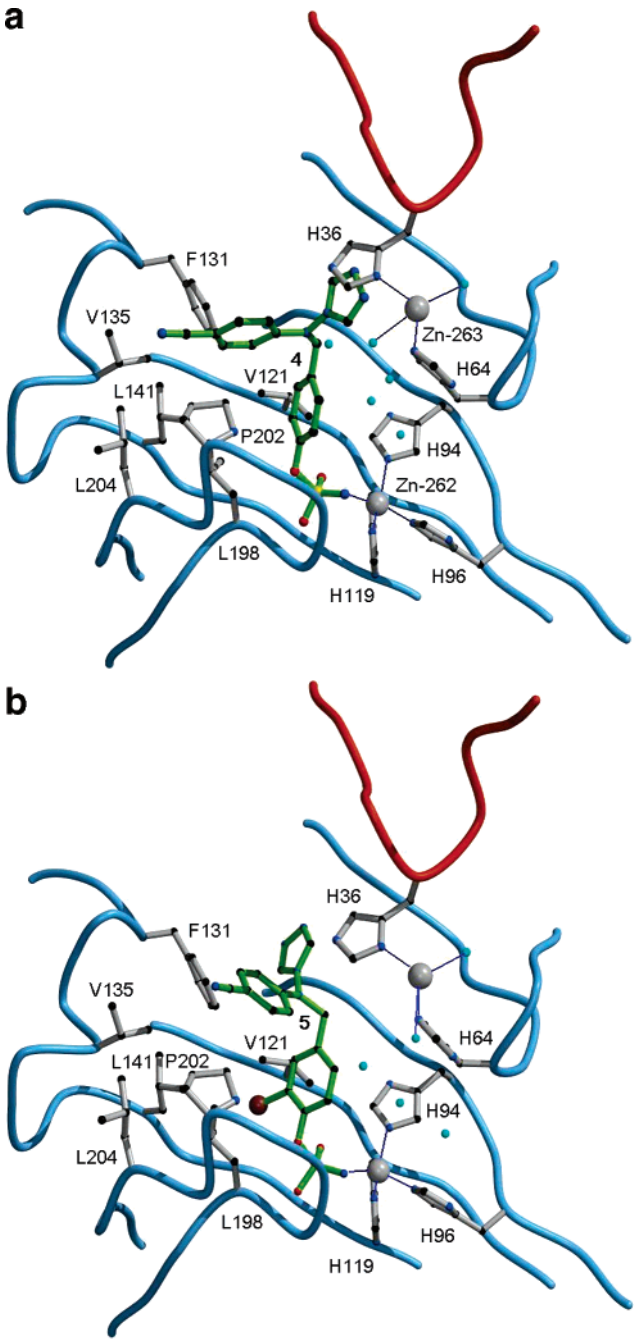

FIGURE 3: Close-up of residues in the active site of CA II binding to (a) **4** and (b) **5**. Secondary structures from the protein molecule are represented by blue coils while those from the symmetry-related molecule by brown coils. Atom colors are gray (zinc), black (carbon), red (oxygen), blue (nitrogen), yellow (sulfur), brown (bromine), and cyan (water molecules). The secondary zinc metal ion from the symmetry-related protein molecule is ligated by His-64 and His-36 (symmetry-related molecule) and is involved in crystal packing interactions. Bonds to metal ions are represented by blue lines. This diagram was prepared using Bobscript (*30*, *31*).

ring is not in the same position as for **4** (Figure 4). Since the triazole and cyanophenyl rings of both **4** and **5** sit within a large funnel on the outside of the protein, it seems unlikely that the difference in stereochemistry is responsible for the difference in binding affinity of these compounds. It is more likely that the observed change in stereochemistry is a consequence of the difference in conformation in the sulfamate-bearing aromatic ring.

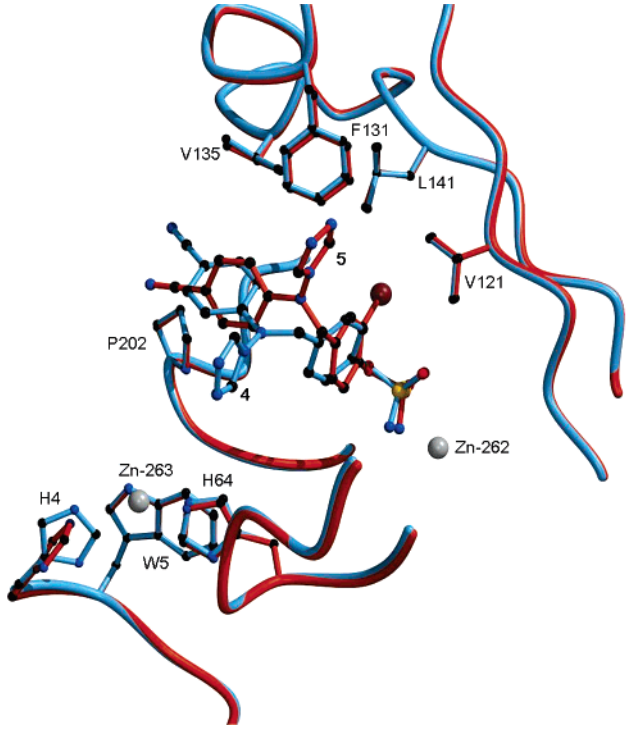

FIGURE 4: Diagram with the structures of **4** (blue) and **5** (brown) overlaid. Atom colors are gray (zinc), black (carbon), red (oxygen), blue (nitrogen), yellow (sulfur), and brown (bromine). This diagram was prepared using Bobscript (*30*, *31*).

Closer examination of the $2|F_o| - |F_c|$ and $|F_o| - |F_c|$ maps reveals that both structures contain positive density orthogonal and close to the sulfamate-bearing aromatic ring (panels a and b of Figures 5 and 6), and this is particularly obvious in the **5** complex. This density is similar in intensity to that expected for a water molecule; however, it is far too close for it to be a water molecule (~1.5 Å), and it is in a hydrophobic region. The origin of this peak is unclear, but it could be due to the presence of a water molecule in a small number of protein molecules without bound inhibitor or may result from an unresolved second conformation of the sulfamate-bearing aromatic ring.

DASI inhibitors were designed so that one molecule could inhibit both the aromatase and STS enzymes, and thus potentially provide dual inhibitory activity against estrogen-dependent cancers. Whether DASI compounds could also exert their anticancer properties by inhibiting other CA isoforms is at present unknown. CA IX and CA XII are overexpressed in cancer, and some good inhibitors of CA II are also good inhibitors of these cancer-related isoforms. Inhibitor **5** is the most potent DASI inhibitor (*12*) but the least potent of the CA II inhibitors tested in this study, with an IC_{50} value 4−5 times higher than those of the most potent inhibitors, including **4**. Some of the key residues (Val-121, Leu-141, Val-143, Leu-198, Pro-202, and Leu-204) interacting with **4** and **5** in the CA II active site are conserved in CA IX and CA XII, as are the zinc binding ligands (His-94, His-96, and His-119). Phe-131 and Val-135 are not conserved in CA IX and CA XII, but these residues sit at the mouth of the wide funnel and probably do not contribute much toward binding of the inhibitors. Further work is required to determine if DASI inhibitor **5** also exerts its anticancer effect by inhibiting CA IX and/or CA XII, but these results in this

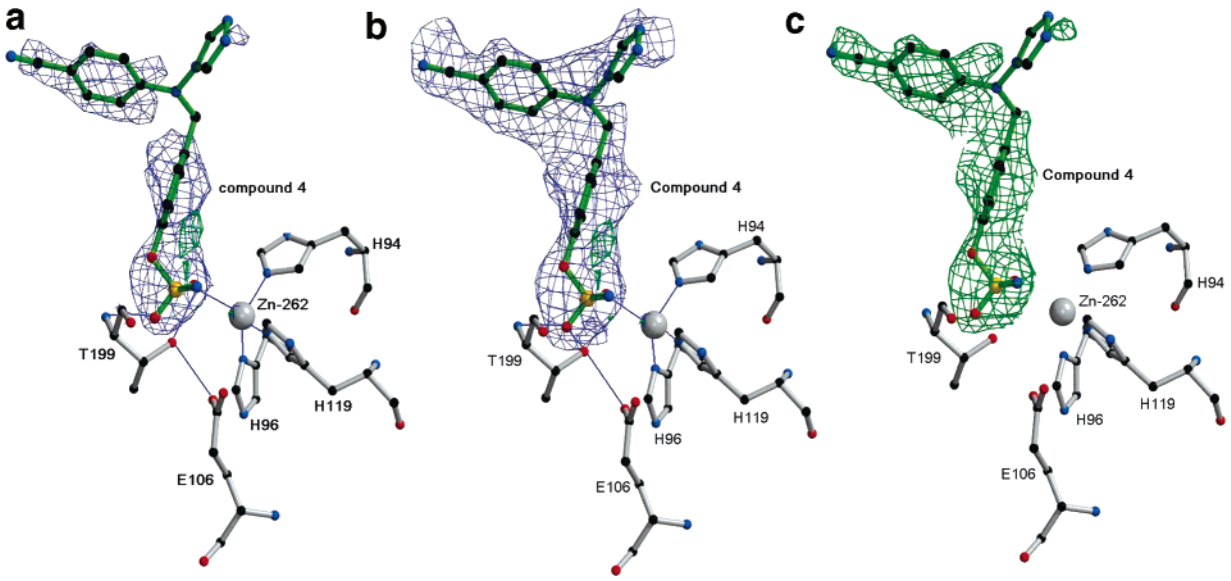

FIGURE 5: Binding of compound **4** in the active site of CA II showing zinc(II) ligation and other interactions. Selected ligand interactions are shown as blue lines, with bond lengths reported in Table 3. Atom colors are gray (zinc), black (carbon), red (oxygen), blue (nitrogen), yellow (sulfur), and brown (bromine). (a) Density for the $2|F_o| - |F_c|$ map (blue) is contoured at 1.0σ, and the $|F_o| - |F_c|$ map is contoured at 3.7σ (green) and -3.7σ (red). (b) Density for the $2|F_o| - |F_c|$ map (blue) is contoured at 0.35σ, and the $|F_o| - |F_c|$ map is contoured at 3.7σ (green) and -3.7σ (red). (c) $|F_o| - |F_c|$ annealed omit map (green) contoured at 2σ. This diagram was prepared using Bobscript (*30*, *31*).

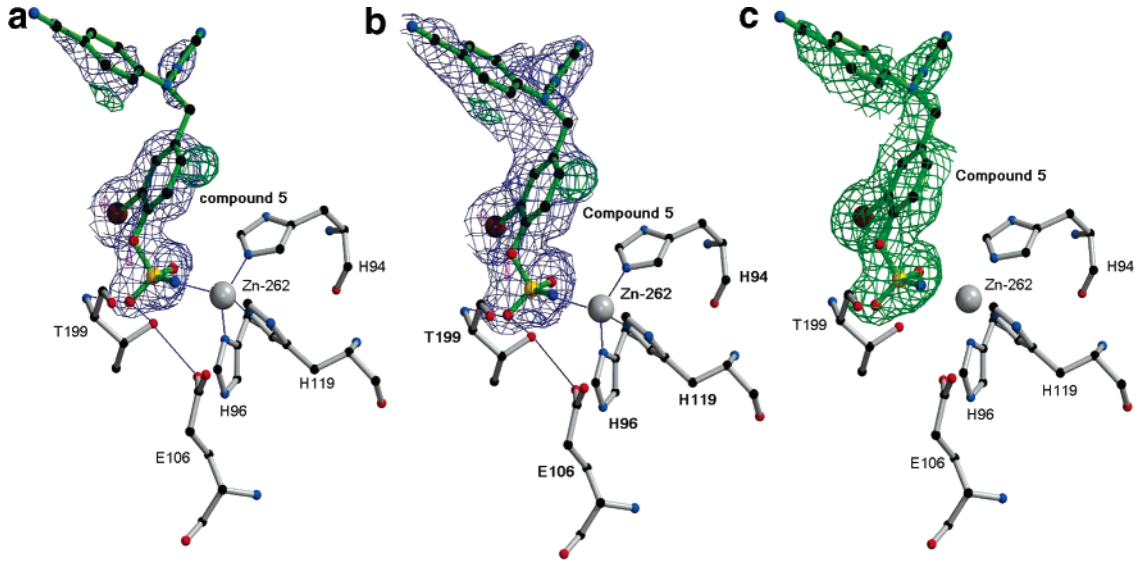

FIGURE 6: Binding of compound **5** in the active site of CA II showing zinc(II) ligation and other interactions. Selected ligand interactions are shown as blue lines, with bond lengths reported in Table 3. Atom colors are gray (zinc), black (carbon), red (oxygen), blue (nitrogen), yellow (sulfur), and brown (bromine). (a) Density for the $2|F_o| - |F_c|$ map (blue) is contoured at 1.0σ, and the $|F_o| - |F_c|$ map is contoured at 3.7σ (green) and -3.7σ (red). (b) Density for the $2|F_o| - |F_c|$ map (blue) is contoured at 0.35σ, and the $|F_o| - |F_c|$ map is contoured at 3.7σ (green) and -3.7σ (red). (c) $|F_o| - |F_c|$ annealed omit map (green) contoured at 1.8σ. This diagram was prepared using Bobscript (*30*, *31*).

paper suggest that inhibition of CA cancer isoenzymes will be of secondary importance.

SUMMARY AND CONCLUSIONS

We have investigated the inhibition of CA II by two prototype DASI inhibitors (YM511-based and letrozole-based) and a related structural variant, and determined the structures of the **4** and **5** complexes by X-ray crystallography. All three of the sulfamate-containing molecules, including a letrozole-based ligand not examined by X-ray crystallography, were modest or good inhibitors of CA II in vitro, suggesting that a wide range of structures can be accommodated within the enzyme active site. As expected, parent aromatase inhibitors **3** and **6** without a sulfamate group were not active as CA II inhibitors. DASIs **4** and **5** in a solution containing predominately DMSO were shown to be significantly more stable than 667COUMATE, the benchmark nonsteroidal inhibitor, and we expect them to be further stabilized in vivo as a result of CA II binding.

Structures of CA II in complex with the best DASI inhibitor, **5**, and the structurally related **4** have been determined. Despite similar chemical structures, several differences in their binding mode are observed, principally in the orientation of the sulfamate-bearing aromatic ring and

the relative orientation of the cyanophenyl and triazole moieties. These results provide a structural basis for the differences in IC_{50} and K_D values for CA II inhibition. The most likely reason for this difference is the displacement of the sulfamate-bearing phenyl ring by the presence of the bromine atom, which in turn may be associated with changes in the configuration of the tetrahedral nitrogen atom. This work also shows that small modifications to inhibitor structures can produce large changes in binding conformation and binding affinity, and underlines the importance of structure-based drug design especially if CA isoform selectivity is desired.

Inhibition of erythrocyte CA II activity is important, inasmuch as this has been shown to be the basis of a novel delivery mechanism for labile drugs (*18*). Binding of sulfamate-based drugs to CA II could be a general method for increasing their stability and relatively efficient delivery and slowing in vivo metabolism. The crystal structures reported here expand our knowledge of the interactions between sulfamate-based ligands and CA II and should stimulate a wider evaluation of the desirable in vivo effects of binding of such compounds to the enzyme.

ACKNOWLEDGMENT

We thank Professor C. Fierke (University of Michigan) for the generous gift of plasmid pACA and Mr. R. Pederick for purifying human recombinant CA II. The Synchrotron Radiation Source at Daresbury, U.K., is acknowledged for beam time and Dr. S. Iyer for help during data collection and refinement. Ms. A. C. Smith is thanked for her technical support.

REFERENCES

1. Maren, T. H. (1988) The kinetics of HCO_3-synthesis related to fluid secretion, pH controls and CO_2 elimination, *Annu. Rev. Physiol. 50*, 695−717.
2. Recacha, R., Costanzo, M. J., Maryanoff, B. E., and Chattopadhyay, D. (2002) Crystal structure of human carbonic anhydrase II complexed with an anti-convulsant sugar sulphamate, *Biochem. J. 361*, 437−441.
3. Casini, A., Scozzafava, A., Mincione, F., Menabuoni, L., Starnotti, M., and Supuran, C. T. (2003) Carbonic anhydrase inhibitors: Topically acting antiglaucoma sulfonamides incorporating esters and amides of 3- and 4-carboxybenzolamide, *Bioorg. Med. Chem. Lett. 13*, 2867−2873.
4. Türeci, Ö., Sahin, E., Vollmar, E., Siemer, S., Göttert, E., Seitz, G., Parkkila, A.-K., Shah, G. N., Grubb, J. H., Pfreundschuh, M., and Sly, W. S. (1998) Human carbonic anhydrase XII: cDNA cloning, expression, and chromosomal localization of a carbonic anhydrase gene that is over-expressed in some renal cell cancers, *Proc. Natl. Acad. Sci. U.S.A. 95*, 7608−7613.
5. Wykoff, C. C., Beasley, N. J. P., Watson, P. H., Turner, K. J., Pastorek, J., Sibtain, A., Wilson, G. D., Turley, H., Talks, K. L., Maxwell, P. H., Pugh, C. W., Ratcliffe, P. J., and Harris, A. L. (2000) Hypoxia-inducible expression of tumor-associated carbonic anhydrases, *Cancer Res. 60*, 7075−7083.
6. Loncaster, J. A., Harris, A. L., Davidson, S. E., Logue, J. P., Hunter, R. D., Wycoff, C. C., Pastorek, J., Ratcliffe, P. J., Stratford, I. J., and West, C. M. L. (2001) Carbonic anhydrase (CA IX) expression, a potential new intrinsic marker of hypoxia: Correlations with tumor oxygen measurements and prognosis in locally advanced carcinoma of the cervix, *Cancer Res. 61*, 6394−6399.
7. Supuran, C. T. (2003) Carbonic anhydrase inhibitors in the treatment and prophylaxis of obesity, *Expert Opin. Ther. Pat. 13*, 1545−1550.
8. Ho, Y. T., Purohit, A., Vicker, N., Newman, S. P., Robinson, J. J., Leese, M. P., Ganeshapillai, D., Woo, L. W. L., Potter, B. V. L., and Reed, M. J. (2003) Inhibition of carbonic anhydrase II by steroidal and non-steroidal sulphamates, *Biochem. Biophys. Res. Commun. 305*, 909−914.
9. Abbate, F., Winum, J.-Y., Potter, B. V. L., Casini, A., Montero, J.-L., Scozzafava, A., and Supuran, C. T. (2004) Carbonic anhydrase inhibitors: X-ray crystallographic structure of the adduct of human isozyme II with EMATE, a dual inhibitor of carbonic anhydrase and steroid sulfatase, *Bioorg. Med. Chem. Lett. 14*, 231−234.
10. Supuran, C. T., Scozzafava, A., and Casini, A. (2003) Carbonic anhydrase inhibitors, *Med. Res. Rev. 23*, 146−189.
11. Woo, L. W. L., Purohit, A., Malini, B., Reed, M. J., and Potter, B. V. L. (2000) Potent active site-directed inhibition of steroid sulphatase by tricyclic coumarin-based sulphamates, *Chem. Biol. 7*, 773−791.
12. Woo, L. W. L., Sutcliffe, O. B., Bubert, C., Grasso, A., Chander, S. K., Purohit, A., Reed, M. J., and Potter, B. V. L. (2003) First dual aromatase-steroid sulfatase inhibitors, *J. Med. Chem. 46*, 3193−3196.
13. Wood, P. M., Woo, L. W. L., Humphreys, A., Chander, S. K., Purohit, A., Reed, M. J., and Potter, B. V. L. (2005) A letrozole based dual aromatase-sulphatase inhibitor with *in vivo* activity, *J. Steroid Biochem. Mol. Biol.* (in press).
14. Howarth, N. M., Purohit, A., Reed, M. J., and Potter, B. V. L. (1994) Estrone sulfamates: Potent inhibitors of estrone sulfatase with therapeutic potential, *J. Med. Chem. 37*, 219−221.
15. Woo, L. W. L., Howarth, N. M., Purohit, A., Hejaz, H. A. M., Reed, M. J., and Potter, B. V. L. (1998) Steroidal and non-steroidal sulfamates as potent inhibitors of steroid sulfatase, *J. Med. Chem. 41*, 1068−1083.
16. Purohit, A., Williams, G. J., Howarth, N. M., Potter, B. V. L., and Reed, M. J. (1995) Inactivation of steroid sulfatase by an active site-directed inhibitor, estrone 3-O-sulfamate, *Biochemistry 34*, 11508−11514.
17. Vicker, N. J., Ho, Y. T., Robinson, J. J., Woo, L. W. L., Purohit, A., Reed, M. J., and Potter, B. V. L. (2003) Docking studies of sulphamate inhibitors of estrone sulphatase in human carbonic anhydrase II, *Bioorg. Med. Chem. Lett. 13*, 863−865.
18. Ireson, C. R., Chander, S. K., Purohit, A., Parish, D. A., Woo, L. W. L., Potter, B. V. L., and Reed, M. J. (2004) Pharmacokinetics of the non-steroidal steroid sulfatase inhibitor 667-coumate and its sequestration into red blood cells, *Br. J. Cancer 91*, 1399−1404.
19. Lloyd, M. D., Pederick, R. L., Natesh, R., Woo, L. W. L., Purohit, A. P., Reed, M. J., Acharya, K. R., and Potter, B. V. L. (2005) Crystal structure of human carbonic anhydrase II at 1.95 Å resolution in complex with 667-coumate, a novel anti-cancer agent, *Biochem. J. 385*, 715−720.
20. Nair, S. K., Calderone, T. L., Christianson, D. W., and Fierke, C. A. (1991) Altering the mouth of a hydrophobic pocket. Structure and kinetics of carbonic anhydrase II mutants at residue Val-121, *J. Biol. Chem. 266*, 17320−17325.
21. Otwinowski, Z., and Minor, W. (1997) in *Methods in Enzymology* (Carter, C. W., Jr., and Sweet, R. M., Eds.) pp 307−326, Academic Press, New York.
22. Scolnick, L. R., and Christianson, D. W. (1996) X-ray crystallographic studies of alanine-65 variants of carbonic anhydrase II reveal the structural basis of compromised proton transfer in catalysis, *Biochemistry 35*, 16429−16434.
23. Brünger, A. T., Adams, P. D., Clore, G. M., DeLano, W. L., Gros, P., Grosse-Kunstleve, R. W., Jiang, J.-S., Kuszewski, J., Nilges, N., Pannu, N. S., Read, R. J., Rice, L. M., Simonson, T., and Warren, G. L. (1998) Crystallography and NMR system (CNS): A new software system for macromolecular structure determination, *Acta Crystallogr. D54*, 905−921.
24. Jones, T. A., Zou, J.-Y., Cowan, S. W., and Kjeldgaard, M. (1991) Improved methods for building protein models in electron density maps and the location of errors in these models, *Acta Crystallogr. A47*, 110−119.
25. Hejaz, H. A. M., Woo, L. W. L., Purohit, A., Reed, M. J., and Potter, B. V. L. (2004) Synthesis, *in vitro* and *in vivo* activity of benzophenone-based inhibitors of steroid sulfatase, *Bioorg. Med. Chem. 12*, 2759−2772.
26. Purohit, A., Vernon, K. A., Hummelinck, A. E. W., Woo, L. W. L., Hejaz, H. A. M., Potter, B. V. L., and Reed, M. J. (1998) The development of a-ring modified analogues of oestrone-3-O-sulphamate as potent steroid sulphatase inhibitors with reduced oestrogenicity, *J. Steroid Biochem. Mol. Biol. 64*, 269−275.

27. Abbate, F., Coetzee, A., Casini, A., Ciantini, S., Scozzafava, A., and Supuran, C. T. (2004) Carbonic anhydrase inhibitors: X-ray crystallographic structure of the adduct of human isozyme II with the antipsychotic drug sulpiride, *Bioorg. Med. Chem. Lett. 14*, 377−341.
28. Abbate, F., Casini, A., Owa, T., Scozzafava, A., and Supuran, C. T. (2004) Carbonic anhydrase inhibitors: E7070, a sulfonamide anticancer agent, potently inhibits cytosolic isozymes I and II, and transmembrane, tumour-associated isozyme IX, *Bioorg. Med. Chem. Lett. 14*, 217−223.
29. Abbate, F., Casini, A., Scozzafava, A., and Supuran, C. T. (2004) Carbonic anhydrase inhibitors: X-ray crystallographic structure of the adduct of human isozyme II with a topically acting antiglaucoma sulfonamide, *Bioorg. Med. Chem. Lett. 14*, 2357−2361.
30. Merritt, E. A., and Bacon, D. J. (1997) in *Methods in Enzymology* (Carter, C. W., Jr., and Sweet, R. M., Eds.) pp 505−524, Academic Press, New York.
31. Esnouf, R. M. (1997) An extensively modified version of Molscript that includes greatly enhanced colouring capabilities, *J. Mol. Graphics 15*, 132−134.

BI047692E